Chapter: 2

Synthesis of Phase Pure $(1-x)Bi(Mg_{3/4}W_{1/4})O_3$-$xPbTiO_3$ Ceramic

2.1 Introduction

Synthesis of pure perovskite phase of $Bi(Mg_{3/4}W_{1/4})O_3$ [BMW] using traditional solid state ceramic method is difficult because of less stable perovskite phase for this compound as the tolerance factor for BMW is quite low (0.884). Solid solution formation of $Bi(Mg_{3/4}W_{1/4})O_3$ with $PbTiO_3$ (tolerance factor = 1.027) stabilizes the perovskite phase for this system but minor impurity phases still appear if the concentration of $PbTiO_3$ is small. As discussed in chapter 1, the phase coexistence region and morphotropic phase boundary [MPB] for $(1-x)Bi(Mg_{3/4}W_{1/4})O_3$-$xPbTiO_3$ ceramics appears for x = 0.62. Thus the perovskite phase of the solid solution system with significant proportion of $PbTiO_3$, in the desired composition range around morphotropic phase boundary, can be prepared by optimizing the synthesis conditions.

In this chapter, we present the details of optimization of synthesis conditions and experimental procedures for the preparation of various compositions of phase pure $(1-x)Bi(Mg_{3/4}W_{1/4})O_3$-$xPbTiO_3$ solid solution. This chapter also presents the brief discussions on the characterization techniques used in the present Ph.D. thesis. Using optimal synthesis conditions for conventional solid state ceramic method, we have prepared pure perovskite phase of $(1-x)Bi(Mg_{3/4}W_{1/4})O_3$-$xPbTiO_3$ solid solution with the compositions x = 0.45, 0.50, 0.55, 0.60, 0.61, 0.62, 0.63, 0.64, 0.65, 0.66, 0.67, 0.68, 0.69, 0.70, 0.72, 0.75 and 1.0. The synthesized samples were characterized for phase purity, microstructural analysis and compositional homogeneity by using powder x-ray diffraction (XRD), scanning electron microscopy (SEM) and energy dispersive spectroscopy (EDS) respectively. Before we present the details of synthesis and sample characterization, a brief overview of characterization techniques used in this work are presented below.

2.2 Characterization Tools

2.2.1 X-ray Diffraction

The x-ray diffraction (XRD) is a powerful technique used to characterize, the phase purity, crystallinity and crystal structure of samples. Powders sample is mounted in a sample holder made by quartz and loaded into the diffractometer for data collection. Phase identification from the XRD data is done by matching the XRD patterns of the materials with the reference patterns from the already available database managed by International centre for diffraction data (ICDD) and similar other sources. Diffraction occurs when there is an interaction between sample and radiation of wavelength comparable to the interplaner spacing of the periodic structure of the crystalline samples. X-rays have wavelengths of the order of a few angstroms which is typical inter-atomic distances in crystalline solids. When X-rays are scattered from a crystalline solid, they can constructively interfere, producing a diffracted beam. X-ray diffraction (XRD) measurements in the present thesis work have been carried out using a 600W CuK_{α} based Rigaku (Japan) Miniflex x-ray diffractometer operating in the Bragg-Brentano geometry and fitted with a curved crystal graphite monochromator in the diffracted beam. The measurements were done at scan speed of 2 degrees/min using scan step 0.02 degree. The XRD data of sintered samples were collected at a scan rate of $1° \text{ min}^{-1}$ in the 2θ range from 10° to 100° at a scan step of 0.02°. High resolution and temperature dependent XRD measurements on some selected samples were carried out by using Rigaku smartLab x-ray diffractometer equipped with Johansson monochromator having $Cu_{k\alpha 1}$ optics.

Bragg's Law:

Bragg's law describes the angle at which a coherent beam of x-rays of a particular wavelength diffracts from a crystalline surface as per the equation below.

$$2d \sin\theta = n\lambda \text{ ……..……..(2.1)}$$

Where ‘λ’ is the wavelength of the x-rays, ‘θ’ is the scattering angle, ‘n’ is an integer representing the order of the diffraction peak and ‘d’ is the inter-planer spacing of periodic structure.

The x-ray diffraction pattern of a given powder sample is obtained by measuring the scattered intensity with the variation of the angle (2θ). Quantitative information on single phase and multi-phase materials can also be obtained using pattern calculation by full diffraction pattern fitting methods. The full diffraction pattern matching analysis by the Rietveld structure refinement, developed by H.M. Rietveld [1969] can determine the most accurate values for sample composition, crystal symmetry, unit-cell dimensions, atom positions, site-occupancy factors and many more information for pure as well as doped samples.

2.2.2 Scanning Electron Microscopy (SEM) and Energy Dispersive X-ray Spectroscopy (EDS)

Accelerated electrons carry significant amount of kinetic energy (KE), which is dissipated due to “electron-sample interactions” producing variety of signals when the incident electrons are decelerated by a sample. In an optical microscope, magnification is obtained by a system of ‘optical lenses’. The smaller is the wavelength of light, the greater is its resolving power which sets a limit over the optical microscope. In electron microscope, wavelength of the radiation can be decreased significantly by changing the accelerating voltage of electron and thereby momentum of the electron matter wave. That is why, despite its smaller numerical aperture, an electron microscope can resolve objects as small as 0.001μ (= 10Å), as compared to 0.2 μ by a light microscope. Thus, the resolving power of an electron microscope is 200 times greater than that of a light microscope.

The microstructure of the calcined powder and sintered pellet surfaces were studied by scanning electron microscopy (SEM) using a Zeiss Evo Research 18. A thin gold film was sputter-coated on the samples before SEM examination. Energy dispersive x-ray spectroscopy (EDS) available with the SEM is used for compositional analysis of the samples. The characterization principle of EDS is that each element has a unique electronic energy state which is the characteristic of that element. So the characteristic x-rays emitted by different elements in the sample are distinguishable from one another due to difference in x-ray photon energy. When an accelerated electron beam is incident on a sample, measuring the energies of the characteristic x-rays emitted by different elements can tell about their relative proportions in the sample.

2.2.3 X-ray Photo-electron Spectroscopy (XPS)

X-ray photoelectron spectroscopy (XPS) is a surface sensitive technique that provides information about the chemical composition, oxidation state (chemical state) of the constituent elements and valance band structure (density of occupied electronic states). XPS is based on the principle of photoelectric effect. When the sample is exposed to mono energetic x-ray photons of energy hν, it emits electrons from the sample surface. The emitted electrons have kinetic energy (K.E.) given by equation (2.2).

$$K.E. = h\nu - B.E. - \Phi \quad \text{.....(2.2)}$$

Where ‘hν’ is the energy of the incident photon, ‘B.E.’ is the binding energy of the electron and ‘Φ’ is the work function. From the above equation, it is clear that photoelectrons can be produced only if $h\nu \geq B.E. + \Phi$ [Stickle (1992)]. The emitted electrons are sorted by their K.E. and the spectrum obtained is a plot of number of emitted electrons per energy interval versus their K.E., known as energy distribution curve (EDC). Since the energy ‘hν’ of the exciting photons is kept fixed, the B.E. of the

electronic states relative to Fermi energy level (E_F) can be determined by measuring the K.E. distribution of the photoelectrons. Therefore, the energy distribution of the photoelectrons corresponds approximately to the energy distribution of electronic states in the solid. The photo-excited electrons may scatter with other electrons, plasmons, phonons, and consequently loose part of their energy so that it may not have enough energy to be able to escape at all and change their momentum. One of the consequences of such scattering is the secondary inelastic background intensity, which becomes dominant at the low K.E., principally due to the electron-electron scattering. Since on an average, a photo electron can travel over a mean free path before being scattered, the electron from a depth of few Å only can reach the detector, making it a surface sensitive technique in spite of large penetration power of the x-rays. Finally, the escape from the solid is possible only for those electrons with a K.E. component normal to the surface that is sufficient to surmount the potential barrier offered by its work function. For photoelectron spectroscopy, three main components are required: (i) a photon source, (ii) an energy analyzer for photoelectrons, and (iii) an electron detector. High vacuum is needed to increase the mean free path of the electrons coming out of the sample surface and reaching the detector, and to reduce the contamination layer covering over the sample surface during measurement. Since the photoelectron energy depends on the source energy, the excitation source must by monochromatic. The energy of the photoelectrons is analyzed by an electrostatic analyzer. For the present study, the X-ray photoelectron spectra (XPS) were recorded by AMICUS (Kratos analytical) x-ray photoelectron spectrometer having a monochromatic MgK_{α} (1253.6 eV) source. During data processing of the X-ray photoelectron spectra, binding energy (BE) values were referenced to the C1s peak (284.6 eV). Quantification of the peaks was performed after Shirley background subtraction using XPSPEAK4.1 software.

2.2.4 Raman Spectroscopy

Raman spectroscopy is the powerful technique to find the types vibrational modes present in materials. The basic requirement of the Raman spectroscopy is that molecule must have the polarizability change. Three different kinds of spectra arise due to interaction of electromagnetic radiation with materials. When the energy of scattered radiation is less than the incident radiation, then it is called Stokes lines while if the energy of scattered light is greater than the incident radiation it is called anti-Stokes lines. The Stokes and anti-Stokes lines arise due to inelastic scattering of photons which comprises the Raman spectrum. The third case is for elastic scattering when the energy of incident radiation is equal to scattered radiation which is called as Rayleigh scattering.

The Raman Effect was first time discovered by Dr. C.V. Raman in 1927. When any molecule is subjected to the electric field the positive charge nuclei of the atoms are attracted to the negative pole field while electrons are attracted towards the positive pole of electric field. This induces dipole moment in the molecule and molecule gets polarized. This can be expressed as $\mu = \alpha E$, where μ is the dipole moment of the molecule, α is polarizability of the molecule and E represents the electric field. The electrical field (E) can be written as: $E = E_o \sin(2\pi\nu t)$, where E_o is the electric field magnitude, ν is the frequency of the electric field. Raman spectroscopy technique can be used to investigate the structure of ceramics by knowing possible stretching band in the molecule. Raman spectra for the present thesis work were recorded using STR-300 spectrophotometer with 532 nm laser excitation wavelength and grating 1200 spectrograph with step size of 1.2 cm^{-1}.

2.3 Experimental Details

Traditional solid-state ceramic method was used to prepare the (1-x)[$Bi(Mg_{3/4}W_{1/4})O_3$]-x$PbTiO_3$ samples at close compositional interval viz. x = 0.45, 0.50, 0.55, 0.60, 0.61, 0.62, 0.63, 0.64, 0.65, 0.66, 0.67, 0.68, 0.69, 0.70, 0.72, 0.75 and 1.0. Analytical reagent grade Bi_2O_3, MgO, H_2WO_4, TiO_2 and PbO of purity greater than 99% obtained from HiMedia Laboratories Pvt. Ltd. were used as raw materials. The reactant powders were characterized by x-ray diffraction before using them. The XRD patterns of Bi_2O_3, TiO_2, H_2WO_4, PbO, and MgO are shown in **Fig. 2.1**. The observed diffraction patterns were compared with the XRD patterns in the ICDD database. The XRD patterns of the reactant powders are in well agreement with that reported in ICDD database [Bi_2O_3, File No. 010709, TiO_2, File No. 894921, H_2WO_4, File No. 780048, PbO, File No. 050561 and MgO, File No. 040829].

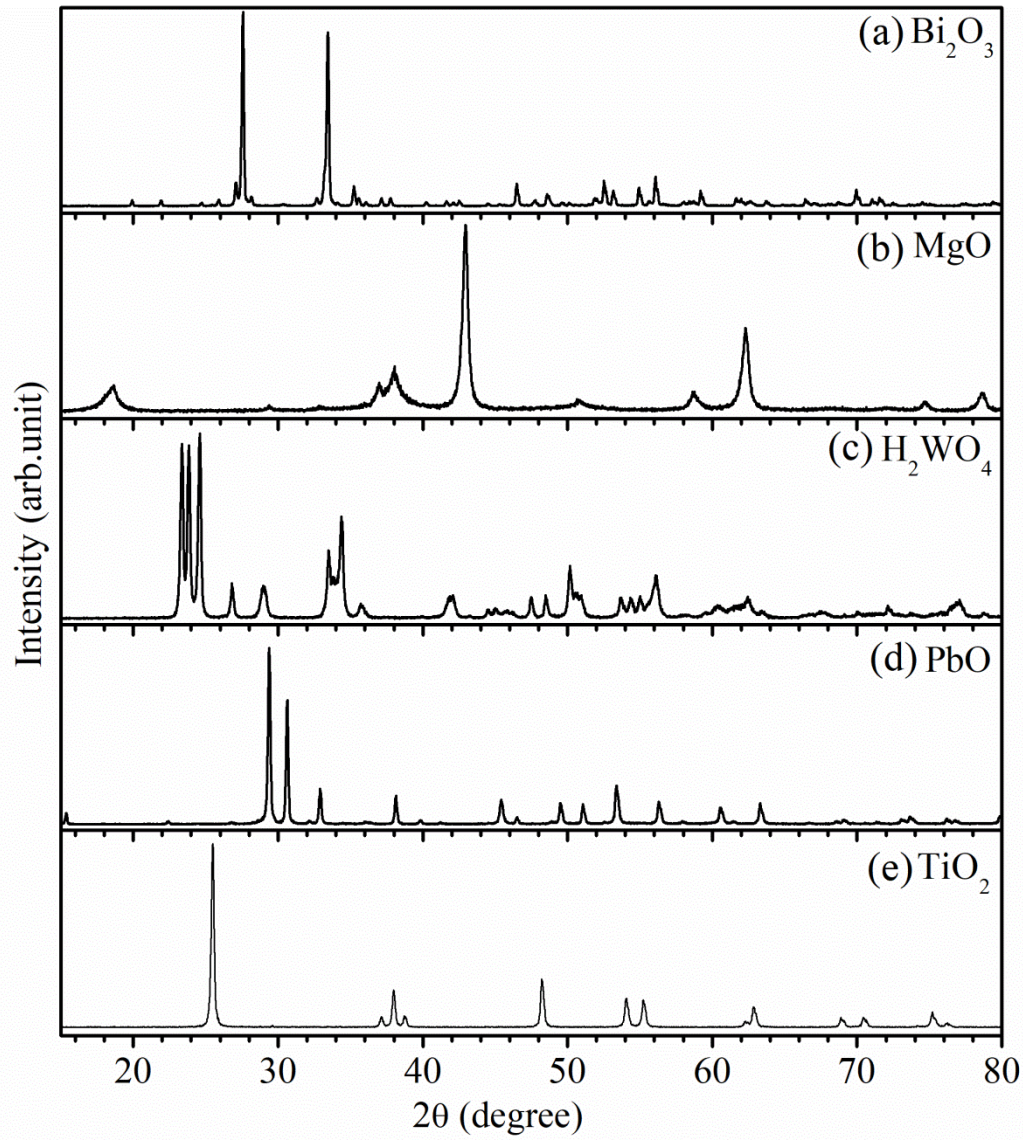

Figure 2.1 Powder XRD patterns of starting ingredients (a) Bi_2O_3, (b) MgO, (c) H_2WO_4, (d) PbO and (e) TiO_2.

2.3.1 Weighing and Mixing

Initial raw materials were weighed in the stoichiometric ratio using analytical balance and properly mixed in an agate mortar pestle for 2 hrs. This mixture was Milled in a planetary ball mill (Retsch GmbH, Germany) for 6 hours using agate jars (500ml) and agate balls of 10mm diameter using analytical reagent grade acetone as mixing medium. The ball-to-powder ratio was 2:1 by weight. The milling was carried out with

the rotation of jars in both the clockwise and counter clockwise directions. After ball milling mixture were dried in open air at room temperature and then calcined inside muffle furnace at different temperatures, to optimize the calcinations temperature/time.

2.3.2 Calcination

Fig. 2.2 depicts the X-ray diffraction (XRD) pattern of (1-x)$Bi(Mg_{3/4}W_{1/4})O_3$-x$PbTiO_3$ ceramics with composition x = 0.62, calcined at temperatures 500^{o}C, 600^{o}C, 700^{o}C, 750^{o}C, 800^{o}C and 850^{o}C for 6 hrs, along with the XRD pattern of pre-calcined powder. The pre-calcined powder and that calcined at 500^{o}C temperature have similar x-ray diffraction patterns, which indicate that chemical reaction does not start at 500^{o}C temperature. The perovskite peaks appear for the calcination temperature of 600^{o}C which suggests that the reaction temperature for the formation of stable perovskite phase is 600^{o}C and above. The perovskite peaks in **Fig. 2.2** are denoted by (P) and impurity phase peaks by *. There is still significant fraction of the unreacted phase at 600^{o}C and therefore we increased the calcination temperature. With increasing calcination temperature the intensity of the impurity phase XRD peaks decreases gradually and stable perovskite phase peaks increases. The fraction of the perovskite phase increases with increasing calcination temperature to 700^{o}C, 750^{o}C, 800^{o}C and 850^{o}C. The XRD patterns shown in **Fig. 2.2**, indicate that nearly single perovskite phase of 0.38BMW-0.62PT ceramic is obtained when the calcination temperature is increased to 850^{o}C. The impurity phase was identified to be Bi_2WO_6 from the ICDD data. The impurity phase fraction was calculated by using the formula % Impurity phase = $(I_{imp.}/I_{perv.}+I_{imp.})x100$, where $I_{perv.}$ and $I_{imp.}$ are the intensity of most intense XRD peaks of perovskite and impurity phases in the sample. It is found to be less than 0.2% for calcination temperature of 850^{o}C. In view of this, optimum calcination temperature for all the compositions of (1-x)[$Bi(Mg_{3/4}W_{1/4})O_3$]-x$PbTiO_3$ is determined to be 850^{o}C for 6 hrs duration.

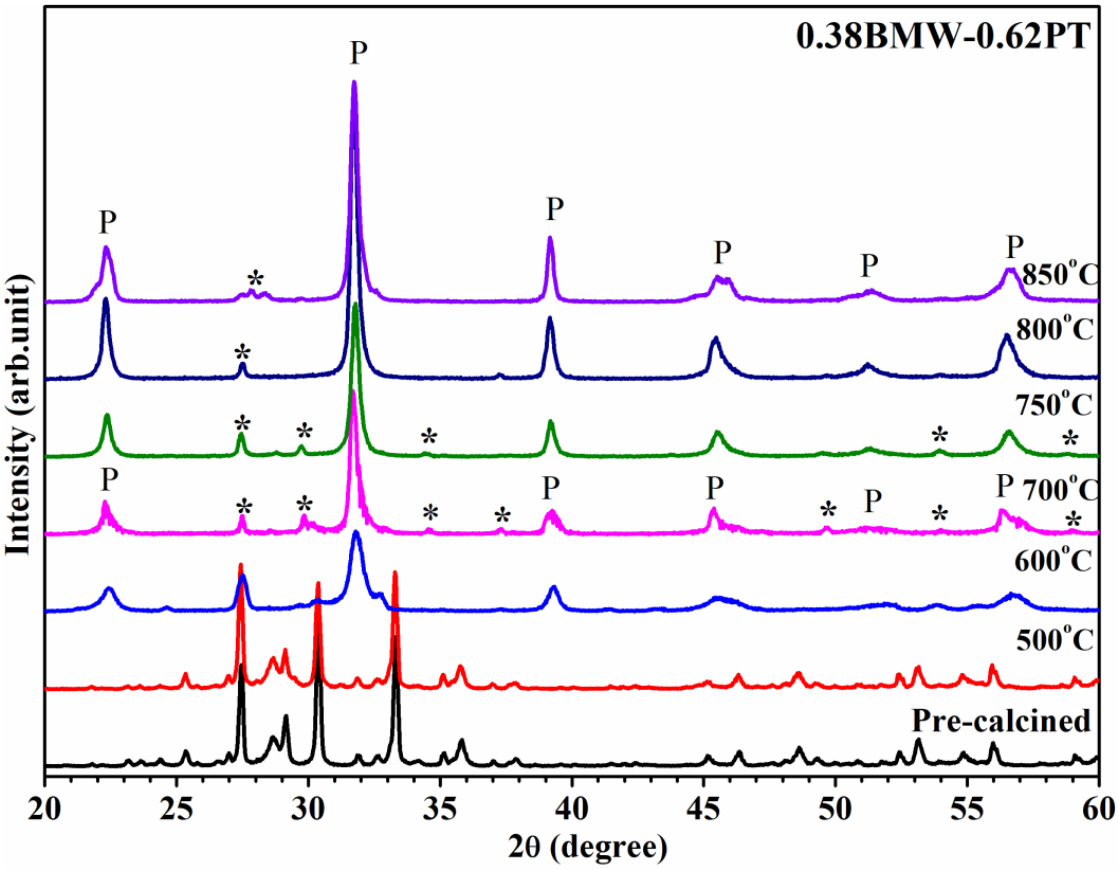

Figure 2.2 Powder XRD patterns of (1-x)Bi($Mg_{3/4}W_{1/4}$)O_3-x$PbTiO_3$ ceramic with composition x = 0.62 calcined at different temperatures 500°C, 600°C, 700°C, 750°C, 800°C and 850°C.

Fig. 2.3 shows the XRD patterns of calcined powders of (1-x)BMW-xPT ceramics with compositions x = 0.45, 0.55, 0.60, 0.61, 0.62, 0.63, 0.64, 0.65, 0.66, 0.67, 0.68, 0.69, 0.70, 0.72 and 0.75 (bottom to top) calcined at 850°C temperatures for 6 hrs. As can be seen from this figure, all the samples are nearly single phase. The compositions with lower concentration of PT have small amount of impurity Bi_2WO_6 phase while higher concentration compositions have very weak signature of the impurity phase.

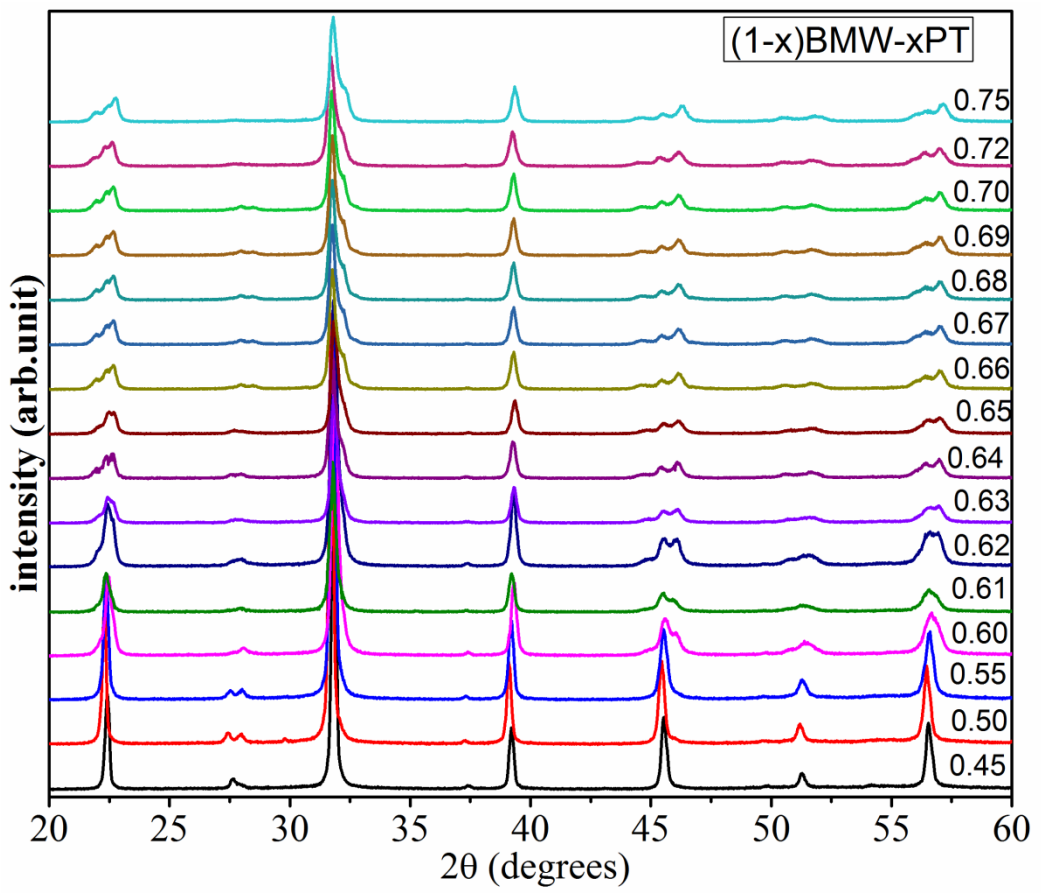

Figure 2.3 Powder XRD patterns of (1-x)Bi($Mg_{3/4}W_{1/4}$)O_3-x$PbTiO_3$ ceramic with compositions x = 0.45, 0.55, 0.60, 0.61, 0.62, 0.63, 0.64, 0.65, 0.66, 0.67, 0.68, 0.69, 0.70, 0.72 and 0.75 respectively calcined at 850^{o}C temperatures.

2.3.3 Preparation of Green Pellets

The calcined powders were crushed into fine powder in an agate mortar for preparation of green pellets. For making pellets, 2% polyvinyl alcohol (PVA) solution in water was used as the binder. The calcined powder was cold compacted using steel die of 12 mm diameter and uniaxial hydraulic press. The load optimization was carried out to overcome the problem of low densification of pellets. After pellet formation, the green density was measured from geometrical dimensions. The optimum load for pellet formation was found to be 75 kN. Thin pellets of around 1 to 1.5 mm thickness were prepared for sintering and further characterizations.

2.3.4 Sintering

Densification of electronic ceramics is a very essential parameter to get the best response. The green pellets were kept in muffle furnace at 500°C for 12 hrs to burn out the binder and then sintered in alumina crucible sealed with MgO powder. The calcined powder of the same composition was kept inside the closed crucible as sacrificial powder for preventing the loss of volatile Bismuth and Lead oxides during sintering. The optimized sintering duration and temperature were found to be 3 hrs and 990°C, respectively. If the sintering temperature was increased above 990°C and sintering time more than 3 hrs, melting of pellets started followed by the formation of impurity phases like Bi_2WO_6 due to loss of Bi_2O_3. After sintering, density of the pellets was calculated by Archimedes principle. The suspended weights of the pellets were measured in distilled water with the help of a special design hanger to hang the pellet inside the distilled water. The density of the sintered pellets was found to be greater than 97% of the theoretical density. Theoretical densities were calculated from the unit cell parameters obtained by XRD study.

Sintered pellets were crushed into fine powders and annealed at 500^oC for 12 hrs before XRD data collection. The XRD patterns of sintered (1-x)BMW-xPT ceramics with various compositions in the range x = 0.45 to 0.75 and pure $PbTiO_3$ are shown in **Fig. 2.4**. All the peaks in the XRD patterns of the sintered powders shown in **Fig. 2.4** could be indexed with the pure perovskite structure except for some small impurity peaks (< 2%) around $2\theta \sim 27^o$-28^o which almost disappear for the higher $PbTiO_3$ concentration. The impurity peaks are due to trace amount of Bi_2WO_6 phase [ICDD Card number-39006]. Since BMW is not a stable perovskite, it is expected that impurity phases will appear for the lower PT concentrations of solid solution.

Formation of very small impurity phase in (1-x)BMW-xPT ceramics in compositions with low PT concentrations is reported by earlier authors also [Snel et al. (2006)].

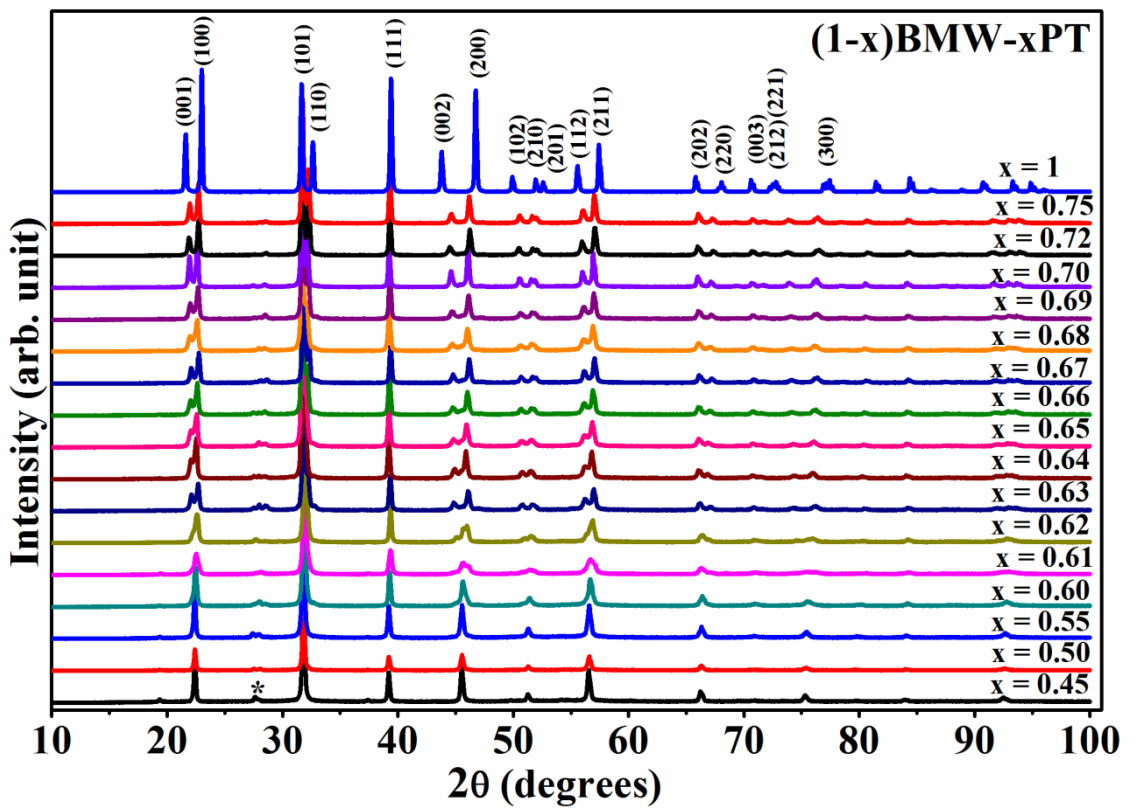

Figure 2.4 Powder XRD patterns of (1-x)Bi($Mg_{3/4}W_{1/4}$)O_3-x$PbTiO_3$ ceramic with compositions x = 0.45, 0.55, 0.60, 0.61, 0.62, 0.63, 0.64, 0.65, 0.66, 0.67, 0.68, 0.69, 0.70, 0.72 0.75 and 1.0 respectively sintered at 990^{o}C temperature.

2.3.5 Microstructure and Compositional Studies

Microstructural studies were carried out on the sintered pellets to determine the grain size, uniformity of the microstructure and chemical homogeneity of the samples. SEM micrograph and EDS spectra of sintered samples of (1-x)Bi($Mg_{3/4}W_{1/4}$)O_3-x$PbTiO_3$ for the representative compositions with x = 0.60, 0.62 and 0.67 are shown in **Fig. 2.5**. The SEM images reveal that the surface morphology is uniform and highly dense. The average grain size was determined from the SEM micrograph using ImageJ

software. The calculated average grain size comes to be ~2 µm. The histogram in the inset to **Fig. 2.5** shows the grain size distribution in the samples. Some larger grains with 3 to 4 µm size are also seen in the microstructure of the composition with x = 0.60 and 0.67. The EDS spectrum in the right panels of **Fig. 2.5** confirms the presence of Pb, Bi, Ti, Mg, W and O in all the three compositions as per the nominal concentrations. No other impurity elements were detected in the EDS analysis.

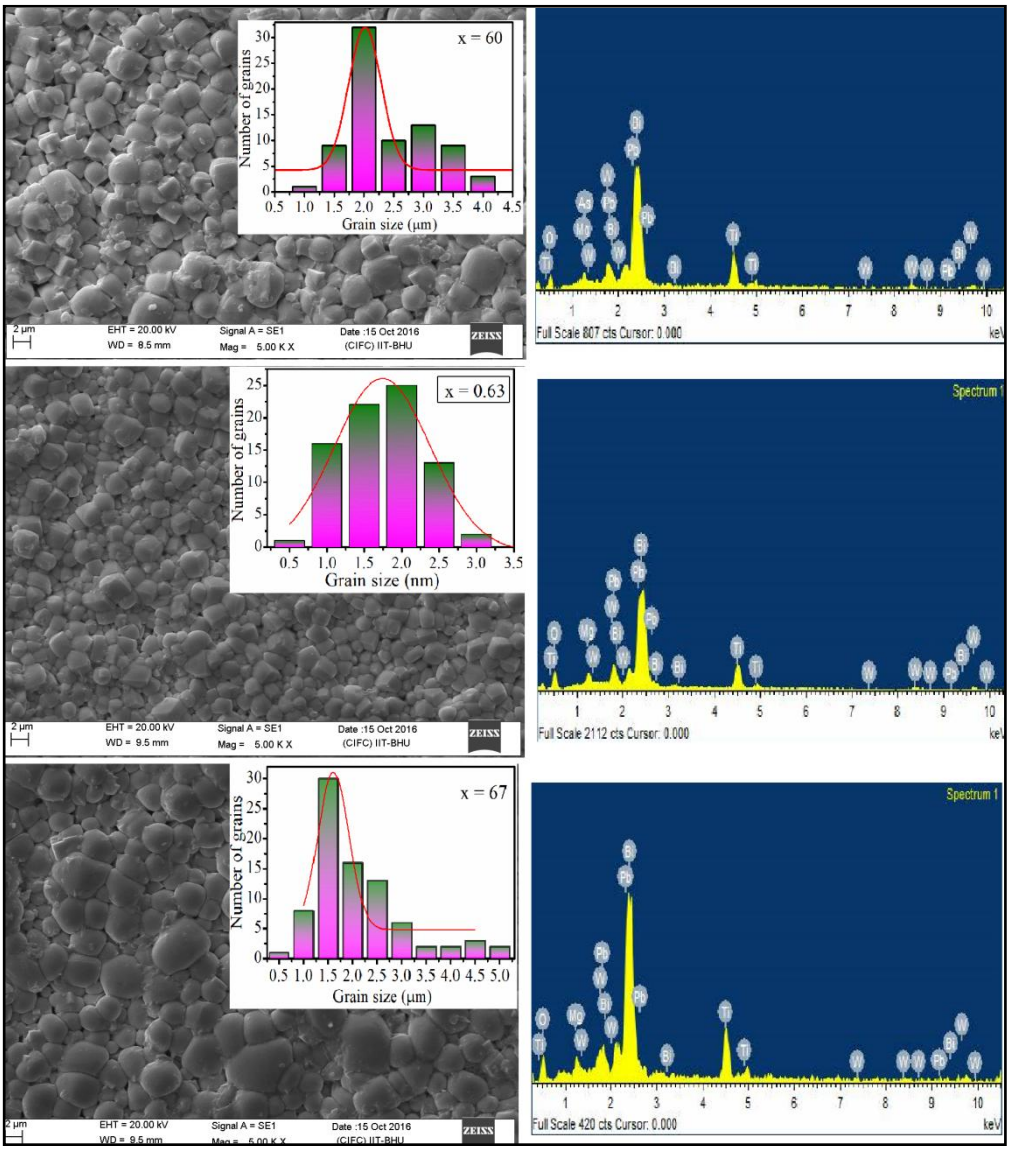

Figure 2.5 SEM images (left panels) and EDS spectra (right panels) of (1-x)Bi($Mg_{3/4}W_{1/4}$)O_3-x$PbTiO_3$ ceramics with compositions x = 0.60, 0.63 and 0.67. The inset histograms show the distribution of grain size in the samples.

Table 2.1 lists the elemental analysis results determined from EDS studies on sintered samples of (1-x)BMW-xPT ceramics with compositions x = 0.60, 0.63 and 0.67. The compositional analysis using EDS results confirms good compositional homogeneity within the experimental error. Since, XRD is not sensitive to detect the light atoms due to low atomic scattering factor, the average atomic percentage of oxygen atom (Z = 8) cannot be determined accurately from the EDS spectrum. This inaccuracy in atomic percentage of oxygen also disturbs the atomic percentages of other atoms (Bi, Pb, Mg, W and Ti).

Table 2.1: Observed and Experimental atomic percentages for (1-x)Bi($Mg_{3/4}W_{1/4}$)O_3-x$PbTiO_3$ ceramics determined from EDS studies.

(1-x)BMW-xPT Composition (x)	Pb		Bi		Mg		W		Ti		O	
	Obs.	Exp.	Obs.	Exp.	Obs.	Exp.	Obs.	Exp.	Obs.	Exp.	Obs.	Exp.
x = 0.60	12	10.7	8	8.97	6	7.59	2	1.60	12	12.16	60	58.9
x = 0.63	12.6	11.6	7.51	9.77	5.55	5.10	1.85	1.55	12.60	12.09	60	63.26
x = 0.67	13.4	12.9	6.6	8.16	4.95	2.47	1.65	2.52	13.40	12.12	60	61.7

2.4 Summary

Nearly pure perovskite phase samples of (1-x)Bi($Mg_{3/4}W_{1/4}$)O_3-x$PbTiO_3$ were prepared by optimized synthesis conditions using conventional solid state reaction method. The optimum calcination temperature for (1-x)Bi($Mg_{3/4}W_{1/4}$)O_3-x$PbTiO_3$ ceramics is found to be 850^oC for 6 hrs duration. The optimum sintering temperature is found to be 990^oC for 3 hrs duration. The average grain size of sintered samples determined from the SEM micrograph is found to be ~2 µm.